Natural Hazards
https://doi.org/10.1007/s11069-025-07303-2

ORIGINAL PAPER

Multidisciplinary investigations of earthflow processes in the differential erosion furrows morphostructural unit, Northern Rif (Morocco): case study of the Seikha landslide

Ali Bounab[1,2] · **Younes El Kharim**[3] · **Rachid El Hamdouni**[4] · **Reda Sahrane**[3] · **Lahcen Ourdaras**[3]

Received: 10 September 2023 / Accepted: 26 March 2025
© The Author(s) 2025

Abstract

In the Rif mountain chain, Slow earthflow processes affectthe clayey and flysch formations of the Tangier and Flysch structural units respectively. To understand the underlying geomorphological processes and the trigger-failure relationship between the local mediterranean climate conditions and the earthflow-like morphologies at the Differential Erosion Furrow (DEF) morphostructural unit, a case study is conducted at the Seikha earthflow. The methodology proposed uses a multidisciplinary approach, coupling in situ geophysical and geotechnical tests to study the geometry of the landslide and remote sensing techniques to monitor its activity. Our results indicate that on one hand, the cross-analysis of geological and geophysical results shows that landslide processes at the study area follow a typical terrestrial-style earthflow model, where the geological structures controlling the landscape's evolution are orientated parallel to the longitudinal stress direction. Vertical and horizontal resistivity variations also allow reconstructing the retrogressive genetic processes responsible for older processes that contributed to the evolution of this hillslope in particular and the DEF morphostructural unit as a whole. On the other hand, the interpretation of multitemporal aerial photographs suggests that the Seikha landslide is in a dormant state and that its acceleration periods follow multiannual cyclic trends related to historic climate and base level fall variations. Seasonal Trends are also emphasized by SBAS (small baseline subset) inSAR (Interferometric Synthetic Aperture Radar) and borehole inclinometer results, which show evidence of slow gravitational deformation that can be accelerated during seasonal rainfall periods.

Keywords Earthflow · ERT · H/V ratio · SBAS InSAR · Northern Morocco

Extended author information available on the last page of the article

1 Introduction

The Rif mountain chain, in Northern Morocco, is characterized by landslides occurrences that threaten the lives and goods of the population (Milliés-Lacroix 1965; El Kharim 2002). Of the various landslide types in the region, complex landslides are abundant, which could be defined as multiple, genetically related "simple" landslides (Varnes 1978; Cruden and Varnes 1996). Such slope instability processes are characterized by the complexity and multigenerational nature of the landsliding, which could be induced by multiple conditioning and triggering factors. Therefore, in order to understand the underlying causes of such landslides, one must investigate their geomorphological and geomechanical evolution as well as their potential triggers.

In fact, lithology is one of the main conditioning factors for earthflow formation, which is generally associated with fine-grained material. In Northern Morocco, earthflow-like landforms are statistically associated with the Tangier and Flysch structural units (Milliés-Lacroix 1965; El Kharim 2002; Mastere 2011; Fonseca 2014), which are characterized by similar facies. Such low-resistance, pseudo-plastic material (Bounab et al. 2021) was modeled by multigenrational slope dynamics since early quaternary times, manifested as translational and rotational slides transforming into earthflows, especially in the central Rif region, where the topography is steeper. In this paper, the latter mass movements are designated earthflows as described by Hungr et al. (2014). In addition to lithology, major geological faulting contributes significantly to the development of such landforms as reported by Bounab et al. (2022) who linked the spatial distribution of complex mass-movements to that of low angle thrust faults that characterize the Rif chain. However, which of the two geological factors is more impactful in the high narrow valleys of the Rif chain is still open to debate. In addition, the complex structure of such landslides, sculpted by the multigenerational slope dynamics of the study area, is not fully documented and understood. Therefore, no inclusive cause and effect model can be established despite the high statistical correlation between certain factors in one hand and complex landslides and large-scale earthflows on the other.

In terms of activity, this type of landslides is globally known by cyclic trends which tend to follow seasonal, annual and multiannual cycles (Iverson and Major 1987; Mackey and Roering 2011), hence, the alternation of dormant state and acceleration periods (Hungr et al. 2014). At present, such large-scale earthflows are dormant or relic in the high narrow Rif valleys. However, El Kharim et al. (2021) and Milliés-Lacroix (1965) showed that old and very old complex landslides in the region could be partially or totally reactivated by (i) extreme rainfall events and/or (ii) rapid, manmade changes to the natural topography.

In an attempt to measure the current displacement rates of some large landsides in the central Rif region, Fonseca (2014) performed the Persistent Scatter SAR interferometry technique (PSinSAR) (Ferretti et al. 2001), on a number of complex landslides. He reported a very low density of Persistent Scatters (PS) and a velocity of 1 to few mm/year in the 2003–2010 period. With this low density and the lack of other studies to complete the observations of this author, further investigations are deemed necessary to enhance our understanding of the trigger-failure relationship between current precipitation regimes and slope dynamics. To do so, a better alternative to PSinSAR is the Small Baseline (SBAS) variation of the same technique (Berardino et al. 2002; Duro et al. 2005; Crosetto et al. 2008),.

In this paper, data on the Seika earthflow are presented as a site-specific case study of a large-scale slope instability that threatens the startigical n°2 national road (RN2) in Northern Morocco. The main focus of this study is exposing the geometry and measuring the current activity rates of the Seikha earthflow using modern field survey, geophysical, geotechnical and remote sensing techniques. The results are used to explain the current trigger-failure relationship in earthflow-like landforms relative to relict and past climate trends. Being located far from a major thrust faults, this earthflow represents a different geological setting to those presented by El Kharim et al. (2021) and Bounab et al. (2022), therefore allowing to complete the observations and findings of these authors.

2 Study area

2.1 Geological and geomorphological setting

The Seikha (which means persistent unstable terrain in local dialect) earthflow is located at kilometer 80 of the RN2 national road in Northern Morocco, at the respective WGS 84 coordinates W=-5.37294 and Y=35.36767. In map view (Fig. 1), it has a typical teardrop shape that characterizes this type of mass movements (Fig. 1). Consequently, it is several times longer than it is wide (approximately 1.6 km long from headscarp to toe and 250 m

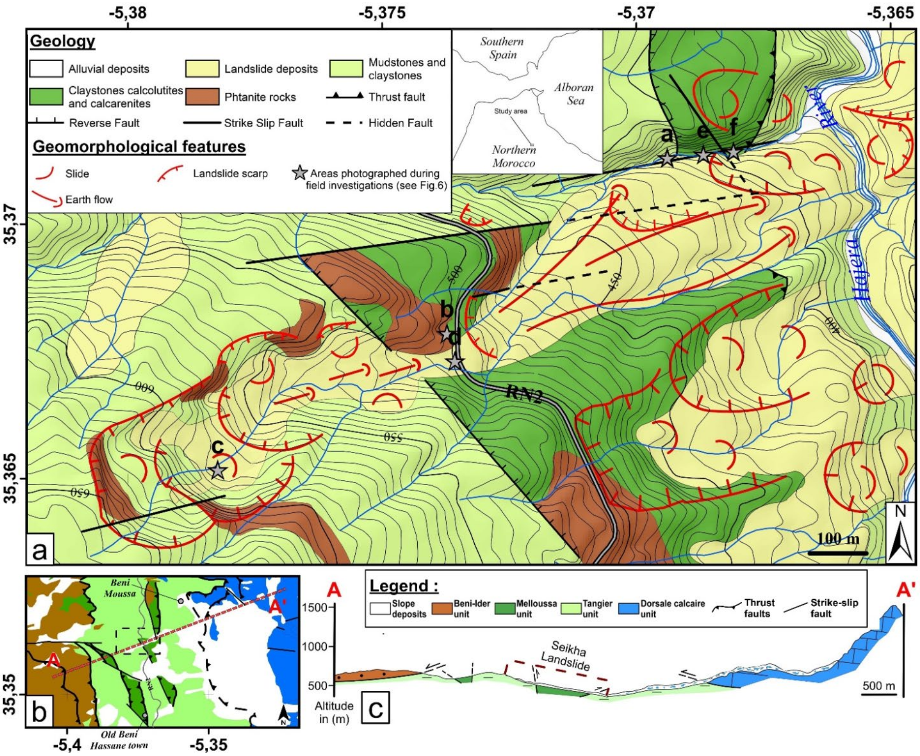

Fig. 1 **a** lithological and geomorphological map of the Seikha landslide. **b** Structural and geological setting of the study area. A-A'– 2D cross-section explaining the geological setting of the Seikha landslide

wide in the depositional area). Its 2D cross-section is characterized by a sinusoidal longitudinal profile, typical of landslides with flow-like morphologies. It affects the hillslope from ridge to thalweg, cumulating an elevation difference of approximately 300 m with a mean slope of around 11°.

This landslide is geologically situated in the External domain of the Northern Rif chain (Didon et al. 1973). From a morphostructural standpoint, it is part of the "Sillons d'Erosion Différentielle" morphostructural unit, defined by El Gharbaoui (1978). This unit, which can be translated as Differential Erosion Furrow or DEF for short, is characterized by N-S oriented, V-shaped valley with deep water incisions (Fig. 1c). The geomorphic processes at the area are mainly controlled by two main groups of discontinuities: (i) N-S to NNW-SSE oriented, West-verging thrust faults (Didon et al. 1973), favoring the development of N-S oriented landforms (El Gharbaoui 1981), and (ii) E-W to ENE-WSW parallel distributed strike-slip faults, compensating for the differential drift velocities (Benmakhlouf 1990; Skakni et al. 2020).

At the Seikha landslide area, a contrast is observed between geological material outcropping to the North and that outcropping to the South, suggesting the presence of the strike-slip faults described earlier (Fig. 1a). At the main track area, a subvertical, NW-SE oriented reverse fault, documented in the 1:50000 official geological map (Didon et al. 2004) separates the two structural units outcropping in the study area, which is associated with the same compressive regime responsible for the N-S thrust faults discussed above. From a lithological point of view, the area where the Seikha landslide occurred is characterized by shale-limestone successions typical of the Melloussa Flysch and Tangier tectonic units presented above. The latter unit is characterized by thicker shale strata with intercalations of phanite layers that mainly outcrop in the head scarp and main track areas of the landslide.

2.2 Climatic setting

The Seikha site is located at the Northern Rif chain, which is characterized at the present time by a sub-humid Mediterranean climate (El Kharim 2002). In the "DEF" morphostructural unit, average annual rainfall maps show that average precipitation values range from 600 to 800 mm/yr, with most rainstorms occurring between November and March (El Kharim 2002). However, the current climate of the region differs from that of early Quaternary times. In fact, being located at the climate boundary between cold regions to its north where glacials were more pronounced, and warm wet region to its South characterized by more liquid precipitations during these periods (current Northern Sahara and Southern Maghreb), the Alboran Sea region suffered from effects of Dansgaard-Oeschger variability especially during Marine Isotope Stage (MIS) 3 and MIS 2 (Fletcher et al. 2008). Hence, one could say that the climate of the study area, as part of this region, was marked by very low temperatures during glacial times and wet warm conditions during MIS5 and at the beginning of MIS1 (Rognon 1987; Fletcher et al. 2008; Candy and Black 2009; Sancho et al. 2015). Therefore, the landforms observed in the Northern Rif are consequential to old and/or relict processes that do not necessarily reflect the present climate conditions. This is crucial to understanding the triggering of such processes in the relatively dry climate of today.

3 Materials and methods

To achieve our aim of understanding the conditioning and triggering factors in DEF unit, we measured the historic and current activity rates and investigated the geometry of Seikha earthflow. The multidisciplinary approach, detailed below, applies modern field investigation, remote sensing, and in situ geophysical and geotechnical techniques to achieve this goal.

3.1 Field investigations

Six field missions were carried out from 2017 to 2021 in order to map landslide features, to monitor its activity and to study its geological fabric. During these surveys, the strike and dip (Right Hand Rule) of 55 tectonic joints were measured in order to determine the main joints direction and its potential relation to the geometry of the landslide body. Results were then presented using a Lambert-projection, Schmidt net and a weighted Rosette projection. To interpret the results in their local setting, the orientation of tectonic structures derived from 1:50000 official geological maps (Didon et al. 2004) were degitized using a Geographic Information System (GIS) tool, and compared to tectonic deformation at the Seikha site. This allows to relate the tectonic structures encountered in the srudy area to their local and regional settings. In addition to joints, bedrock outcrops were further investigated for the presence of other tectonic structures such as faults and folds that can be responsible for shaping the landslide's morphology.

3.2 Interpretation of multi-temporal, aerial photographs

In the study area, aerial photographs dating back to 1955, 1958, 1965, 1986 and 2010 were studied and compared to google earth satellite images of 2013 and 2019. Although simple in principle, this method of comparison between old and new remotely sensed photographs allows to partially reconstruct the history of a given landslide and to better understand its kinematics especially in undocumented areas where reliable information is scarce.

3.3 Geophysical investigations

Two types of in situ geophysical tests were performed at the study area.

The first is Electrical resistivity Tomography (ERT), which is commonly used to study the subsurface geometry of landslides (Jongmans and Garambois 2007; Perrone et al. 2014). In the case of the Seikha landslide, we exploited the resistivity contrast between the water-rich earthflow deposits and the underlying claystone material, in order to determine the depth of the slip surface and to characterize the subsoil structure. In May 2018, after 4 months of rain, 19 ERT profiles were performed with an 11 electrode overlap, which were arranged and concatenated into 8 2D geo-electrical profiles covering the totality of the landslide-affected area (Fig. 2). These profiles were conducted using a 32 electrodes ER tomograph. We used the maximum inter-electrode spacing value for our device (5 m) in order to reach deep strata. The configuration used was Wenner's because of the relatively small current magnitudes needed to produce measurable potential differences and the sensitivity of this configuration to near surface inhomogeneities (Mooney and Wetzel 1956).

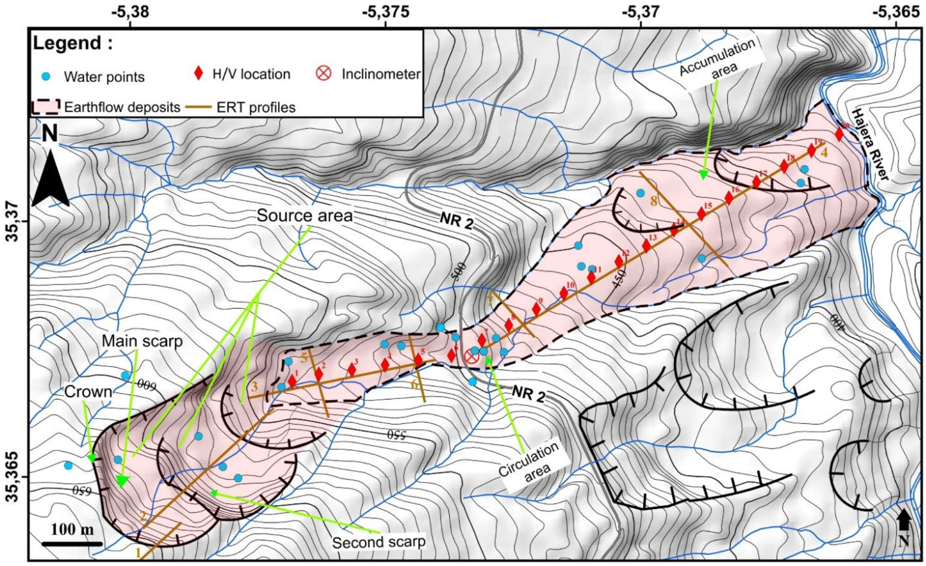

Fig. 2 Map showing the location of water points, and in situ geophysical and borehole inclinometer tests conducted at the area

To perform the data inversion, Res2Dinv commercial software was used. It is based on the conventional smoothness constrained least square method: L2-norm (Degroot-Hedlin and Constable 1990; Sasaki 1992; Loke et al. 2003).

The second geophysical technique used is the H/V single station technique which was originally developed by (Nakamura 1989) for micro-seismic zoning applications. In spite of its ability to reveal resonance properties in complex settings such as unstable or marginally stable slopes, it has rarely been employed as a method to reliably detect the slip surface of landslides (Gaudio et al. 2014; Pazzi et al. 2017).

The H/V technique measures indirectly the density and coherence contrasts between soil layers overlying a hard substratum. (Lermo and Chavez-Garcia 1994; Wathelet et al. 2004; Bonnefoy-Claudet et al. 2006; Gaudio et al. 2014). Using Eq. 1, the depth of this stratigraphic boundary (h) can be calculated provided that the average shear wave velocity (V_s) is known, which is very useful for landslide investigations as a whole and earthflow case studies in particular.

$$f0 = \frac{V_s}{4h} \tag{1}$$

In the study area, 20 H/V measurements were performed using 4 Tromino®, an all-in-one compact 3-directional 24-bit digital tromometer developed by MoHo s.r.l. The duration of each measurement was set to 20 min with a sampling frequency of 128 Hz. The distance between each 2 stations was set to approximately 50 m, forming a longitudinal profile parallel to the direction of longitudinal stress. This allows measuring the H/V peak variations as a function of the runout distance. A 2D profile can subsequently be produced using Eq. 1 (Pazzi et al. 2017). To obtain V_s values of the soft earthflow deposits, the borehole inclinometer data were used to obtain the h value at the borehole location, which corresponds to the depth of the slip surface. Then Eq. 1 was used for the computation of V_s.

3.4 Climate data

In the study area, annual precipitation data of the last century measured at the Torreta meteorological station (X=5° 22’ 18” W; Y=35° 33’ 33” N), were compared to the results of multi-date aerial photograph interpretation, in order to look for a possible correlation between annual climate cycles and landslide acceleration events documented by historic aerial photograph missions. This meteorological station was chosen because of its long hydrometric record which covers 90% of the twentieth century, thus allowing for a wider observation window.

Regarding daily rainfall, data from the Koudiat Kourirène meteorological station (X=5° 10′ 38.97″W; Y=35° 21′ 40.87″N) were used because of its proximity to the landslide (located 15 kms to the E of the study area). The results were confronted with borehole inclinometer and SBAS interferometry results so as to examine potential seasonal rainfall effects on the landslide’s activity.

3.5 Borehole inclinometer monitoring

The borehole inclinometer technique is a well-known in situ geotechnical test that measures relative cumulative displacement as well as the exact depth of the slip surface in a given landslide, provided that the borehole reaches depths greater than that of the slip surface or the mobilized zone (Borgatti et al. 2006; Calcaterra et al. 2012; Marschalko et al. 2012). For accessibility reasons, only one, 30 m deep inclinometer borehole was executed in the Seikha landslide’s main track area (Fig. 2). The borehole was surveyed from December 2017 to May 2019. After this date, no more measurements could be performed because of the borehole closure.

3.6 Unmanned aviation vehicle survey (UAV)

UAV surveys have recently been increasingly used in the field of landslides and more generally in the context of high-precision geomorphological surveys (Brückl et al. 2006; Niethammer et al. 2012; Turner et al. 2015; Rossi et al. 2018; Gracchi et al. 2022). It gives the ability to produce very high-resolution topographic data using structure-from-motion photogrammetry. In this study, UAV photographs were exploited to generate a very high-resolution Digital Surface Model (DSM; 11 cm per pixel) and ortho-image. Here, the results were only used to precisely map landforms and to produce topographic input data for ERT inversion. Acquisition parameters and hardware specifications are indicated in Supplementary, Table S1.

3.7 SBAS interferometry

Among the different MT-InSAR techniques, the one referred to as Small BAseline Subset, SBAS (Berardino et al. 2002; Lanari et al. 2007; Manunta et al. 2019) has been used here. This method relies on an appropriate combination of differential interferograms produced by data pairs with small temporal and spatial baselines in order to limit decorrelation effects (Zebker and Villasenor 1992). It has demonstrated an accuracy of 5–10 mm (time-series) and 1–2 mm / year (velocity), (Manunta et al. 2019).

To perform (SBAS) interferometry, a network of 38 Sentinel 1 Single Loop Complex SAR products (Supplementary, Fig. S1) were processed using the snap-stamps processing chain (Hooper et al. 2012; Foumelis et al. 2018). The chosen scenes were download from the Alaska Satellite Facility platform (https://search.asf.alaska.edu/) and were all acquired in ascending geometry given the aspect of the landslide slope.

In addition to the fact that Sentinel images are freely available, their main advantage is their high spatial resolution (around 12 m) and acquisition frequency (6 to 12 days), which can be adapted to various applications. In this research, the images used covered the period from 06/10/2017 to 11/05/2019, which is the same survey period for the borehole inclinometer technique. The maximum temporal and vertical baselines were set respectively to + 60 days and 150 meters (Supplementary, Fig. S1). Such relatively small baseline value allow to obtain coherent interferograms, hence more accurate and dense measurement (Berardino et al. 2002; Duro et al. 2005; Crosetto et al. 2008). The digital elevation model (DEM) used for interferogram computation is a high resolution 10-m DEM, generated from topographic contours (1/25 000 topographic maps of 2010).

Since clouds and other atmospheric phenomena tend to produce phase delays, the latter need to be filtered in order to obtain precise ground displacement measurements (Lemoine et al. 1995; Zebker et al. 1997; Li et al. 2006). To do so, the TRAIN software (Bekaert et al. 2015) was used.

4 Results

4.1 Field surveys

In the field; a lithological contrast between the undisturbed bedrock material and the reworked slowly deforming, earthflow deposits is evident (Fig. 3a). Slow constant displacement is manifested by fracturing and deformation observed in the old retaining wall, which was constructed after the main events of 1955–1956, and the road subsidence affecting the new recently repaired asphalt (Fig. 3d). In the crown area, where phtanite material outcrops, recent excavations related to quarrying discovered old centimetric layers of scree deposits at the main and secondary scarps. Back tilted blocks of rotated phtanite layers are seen, which demonstrates the rotational activity of the landslide uphill. Below the secondary scarp, fresh, non-weathered clayey material is uplifted during acceleration periods of the last century (Fig. 3c), which could also be observed immediately below the RN2 segment. At the main track, where the landslide's is noticeably narrower, a higher concentration of phtanite layers is found. This thickening is caused by the presence of a NNE-SSW oriented hinge zone corresponding to the folding of phtanite layers (Fig. 3b). At the landslide's lateral boundaries, where water incision is deeper and fresh bedrock material outcrops, E-W geological strike-slip faults and slickensides are found (Fig. 3a, e, f).

The projection of faults strike directions on Schmidt-net (Fig. 4) shows that, on a local scale, two major types of structures are to be distinguished (Fig. 4b, c): (i) NNW-SSE oriented thrust faults and (ii) ENE-WSW strike-slip faults compensating for the differential

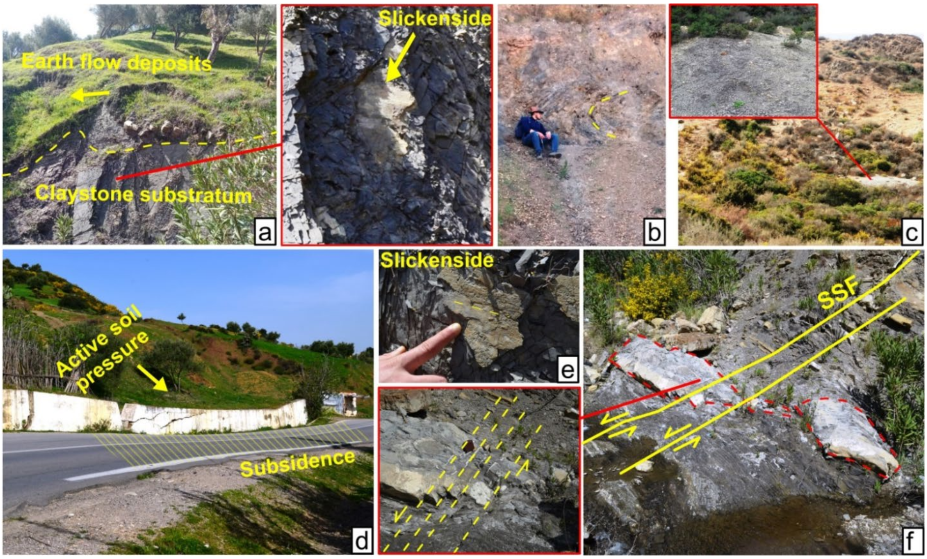

Fig. 3 Photographs taken during field investigations (see Fig. 1 for location), featuring the soil-bedrock boundary (**a**), folding at the main track area (**b**), recent clayey material uplifted by earthflow processes (**c**), road subsidence and landslide-induced damage (**d**), slickensides (**f** and **e**) and strike-slip faults (SSF) found at the study area

crustal deformation. At the Seikha site, tectonic joints are orientated following three main directions: NNE-SSW, NE-SW and NW-SE (i.e. parallel to the longitudinal stress direction) (Fig. 4a, d). The first joint groups (J1 and J2) constitute a very dense conjugate system (Fig. 4), while the third (J3) is orthogonal to the first two with joint planes mainly dipping towards the NE. Strike slip faults and slickensides observed in the field (Fig. 3e, f) are oriented E-W, which is similar to local scale results.

4.2 Landslide geometry interpreted from the geophysical and geotechnical results

By referring to the (Palacky 1988) resistivity scale of the main earth materials, two subsoil layers can be identified in the 2D ERT profiles (Supplementary, Fig. S2): a low resistivity water rich upper layer (R<40 ohm.m) and a higher resistivity underlying layer (R>40ohm.m). The first one corresponds to the earthflow deposits while the second is the claystone substratum.

In the longitudinal profiles (P1, P2, P3 and P4) (Supplementary, Fig. S2), the boundary between these two layers is irregular. In the crown area, its morphology is stepped, which can be explained by the rotational deformation affecting this part of the landslide. At an elevation of 840 m, the high resistivity layer (Substratum) outcrops, which agrees with our field observations. Downhill, the separation surface is smoother, especially in the main track area (P3) (Supplementary, Fig. S2), where its depth ranges from 10 to 20 m. In the depositional area, P4 (Supplementary, Fig. S2) shows that the low resistivity layer becomes thicker (20 to 30 m) especially near the landslide toe area.

Despite the smoothness of this boundary, ridges are observed: the first one is located at the 170 m mark and the second one is found at the 560 m mark (P4) (Supplementary, Fig.

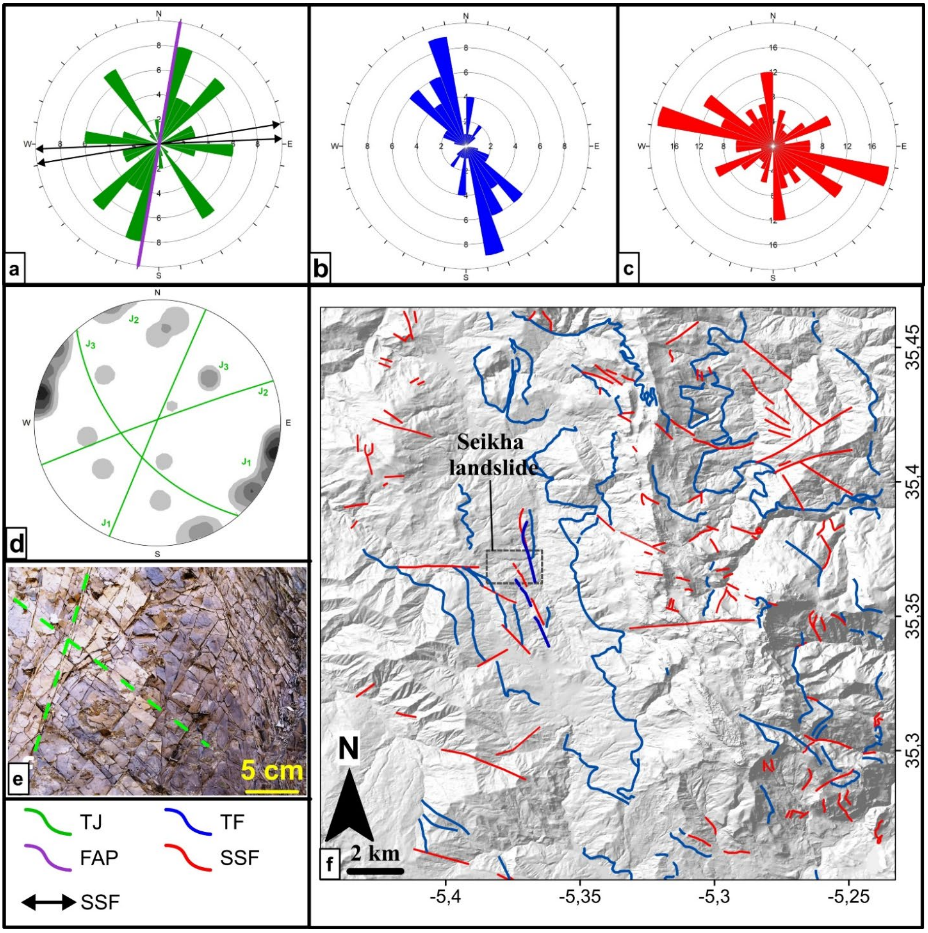

Fig. 4 Stereographic projections of geological structures. **a** Weighted rosette projection of tectonic joints (TJ) at the study area showing strike-slip faults (SSF) and fold axial plane (FAP) strike. **b** Weighted rosette projection of local scale strike-slip (SSF) structures. **c** Weighted rosette projection of local scale thrusts and reverse faults (TF) structures. **d** Main joints directions measured in the Seikha site. **e** In field photograph showing the dense joints network affecting the bedrock material. **f** Map showing structures used in local scale analysis

S2). The origin of these forms and their genetic relationship with the complex landsliding at the study area are discussed in Sect. 5.2.

In the transverse profiles (P5 to P8) (Supplementary, Fig. S2), the same results are obtained regarding the vertical resistivity variations where both previously described layers are observed. The shape of the earthflow deposits, as determined by the resistivity values, is well aligned with the morphology of the landslide (landslide deposits narrower in the main track and wider at the depositional area). In profile 8, we observe a significant elevation difference in the soil-bedrock boundary at the 120 m mark, which further supports the presence of a strike slip fault buried under the landslide deposits.

The spatial distribution of the H/V single station measurements is shown in Fig. 2. In total, 20 stations were put in place which cover most of the landslide-affected area. In stations 6 and 11, a natural peak is observed at roughly 2.2 to 2.4 Hz (Fig. 5a, b), which results from a contrast in lithology, porosity and interstitial fluids between earthflow deposits and their substratum. In other stations, similar peaks are found, the position of which varies depending on the thickness of the earthflow deposits and its density. Secondary peaks, although present in most stations, are ignored in this study since our main objective is to determine the depth of the slip surface and not the study of deeper stratigraphic boundaries.

From single station measurements, an ENE-WSW 2D profile was constructed (Fig. 5c). It allows visualizing H/V ratio peak variations as a function of runout distance. In our case, the H/V peak frequencies range from around 1.5 Hz to 5 Hz. Assuming that the earthflow deposits of the Seikha landslide are homogenous; these variations allow calculating the depth of the slip surface alongside the earthflow longitudinal profile.

For station 7 (the closest to the borehole inclinometer) the H/V peak is located at 1.69 HZ. Since the depth of the slip surface is h = 14.5 m according to borehole inclinometer results, the average V_s value for the landslide deposits is estimated at 104 m/s. Knowing this, the depth of the sliding surface and its geometry were reconstructed from single station peak H/V values by subtracting h from each station's elevation. The latter value was derived from the high-resolution UAV DSM. The results show that the slip surface is irregular in the main track area, with a depth varying from 10 to 20 m (Fig. 5c). In the depositional area, its geometry is smoother. Its depth is in fact constant (around 15 m) from the 500 m to the 800 m mark. At the landslide's foot, its depth is greater (>30 m).

4.3 Temporal evolution

From the interpretation of aerial photographs, we see that the Seikha landslide already existed before 1955. However, a substantial and perceptual displacement is observed in the 1955 photograph (Supplementary, Fig. S3), which corresponds to the infamous 1955 event that caused the complete shutdown of RN2 national road. During the event, the road

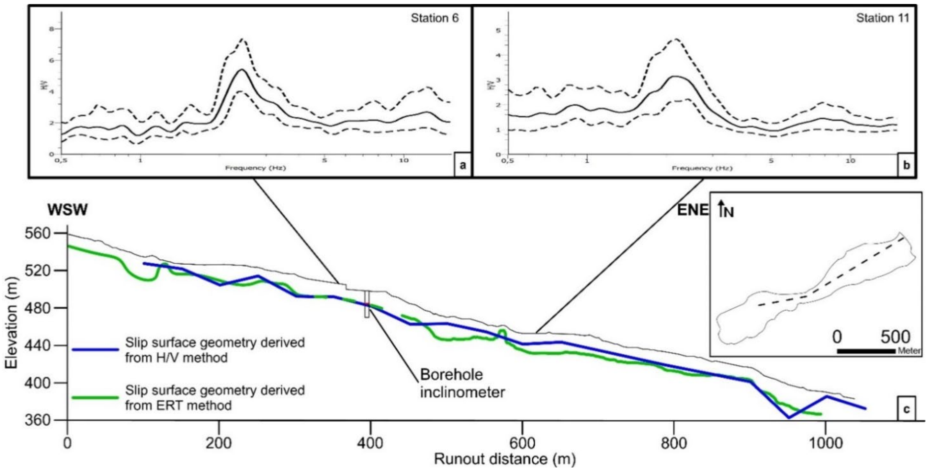

Fig. 5 Comparison of the slip surface geometry reconstructed using ERT and H/V ration methods

segment passing through the landslide was pushed 10–15 m downhill according to our field surveys. In 1958, the landslide was still partially active with the displaced area becoming wider (Supplementary, Fig. S3). In the 1965 aerial photograph, the partial reactivation is mainly perceptible in the secondary scarp. The material displaced did not however reach the main track where the road segment is located. This indicates that the Seikha landslide is enlarging in the zone of depletion where fine-grained material is more abundant. Also, in the foot area, perceptible deformation is observed in the 1965 photograph where slow, but significant earthflow deformation started to push material downhill. From 1965 to 1986; the road segment was constantly repaired and no more significant damage was observed. However, the ravine that delimits the landslide to the North has been subject to strong uneven erosion caused by the slow, permanent creep of the earthflow mass to the NE due to the reactivation of the foot area (Supplementary, Fig. S3). From 1986 onwards, no major changes are observed.

A comparison of the date of the above-detailed results with the annual precipitation values recorded for the 20th century reveals a good correlation between acceleration periods and strong precipitations (Supplementary, Fig. S3). For instance, the 1955 event corresponds to a rainy wet season with precipitation values exceeding the 1000 mm mark. Also, similar conclusions can be drawn for the next year should be responsible for the latter deformation observed in the 1958 aerial photograph. The acceleration seen in the 1965 photograph is associated to a multi annual extreme precipitation period (1963–1966). From this date onward, no significant deformation is observed despite the extremely rainy period of 2000–2010.

4.4 Current displacement rates

4.4.1 Borehole inclinometer results

The borehole inclinometer executed in the study area confirms the current slow processes affecting the earthflow deposits. Figure 6a shows that relative cumulative displacement during the survey period (11/2017 to 04/2019) is in excess of 12 mm downhill, which corresponds to an annual rate of approximately 1 cm/year. The deformation recorded affects

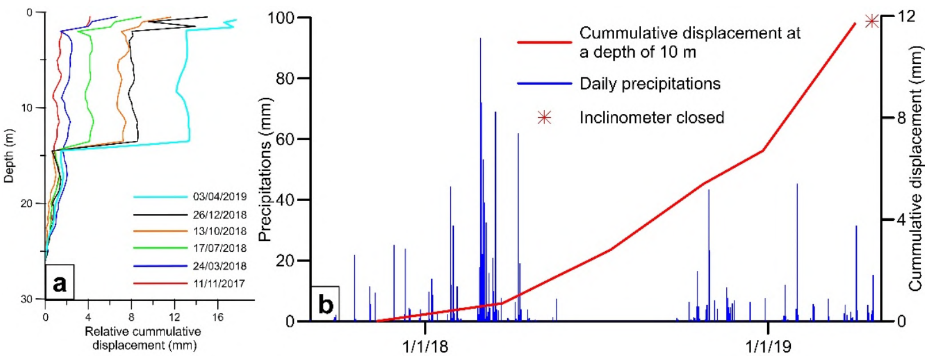

Fig. 6 Borehole inclinometer results. **a**. Relative cumulative displacement recorded during the survey period. **b**. cumulative displacement curve at a depth of 10 m, plotted against daily precipitations data of the Kourirene meteorological station

deposits down to 14.5 m deep. Below this depth, no more displacement is measured. This indicates that the slip surface is reached. The relative cumulative displacement at a depth of 10 m and daily rainfall data plotted against time (Fig. 6b), show that the exceptionally rainy winter of 2018 triggered an acceleration of the landslide, which stayed active until the closure of the borehole in May 2019.

4.4.2 SBAS interferometry results

The PS density obtained in the study area using SBAS-inSAR (Fig. 7b) is significantly better compared to PS-inSAR results with the same input data, where no PS is calculated inside the landslide boundary (Fig. 7a). In terms of deformation, SBAS results show that the maximum downhill displacement rate (negative values) reaches 14 mm/yr, with most of the subsidence observed being spatially correlated with landslides geomorphological features. This depth corresponds to the stratigraphic boundary between the undisturbed substratum and the reworked material as indicated by core samples extracted during the execution of the borehole. While the displacement calculated using SBAS interferometry is sub 1 cm/yr, the maximum deformation is observed in the main track where the velocity exceeds this value. In point 1 (Fig. 7-b) which is the closest to the borehole inclinometer, the calculated deformation rate (11 mm/yr) is similar to that measured in the borehole at a depth of 10 m.

The deformation time series (Fig. 7c) for points 1, 2 and 3 (see location in Fig. 7b) show a good correlation between landslide deformation rates and seasonal precipitations, since the displacement was accelerated after the exceptionally rainy winter and spring of 2018.

5 Discussion

5.1 Limitation of the study

The resistivity contrast obtained in this study is deemed very useful in determining the depth of the basal slip surface. Similar results were found by authors working on earthflows where vertical and horizontal resistivity variations allowed to determine the exact position of the lithological boundary separating reworked, less resistant material constituting the earthflow body, and the underlying bedrock layers (Perrone et al. 2014; Prokešová et al. 2014; El Kharim et al. 2021).

As for the H/V technique, the f_0 values obtained from single station measurements were successfully used for the reconstruction of the slip surface geometry using the borehole inclinometer results as a reference technique. A comparison between the geometry of the basal slip surface obtained from both geophysical methods used in this study is given in Fig. 5. It shows that the morphology obtained using both approaches is similar (Fig. 5). Given the higher density of real data points used for the ERT inversion, it can be used as reference to evaluate the reliability of the H/V technique in determining the depth of landslides separation surfaces. Accordingly, the accuracy of the H/V method is found to be reasonable. However, a significant difference is observed from 500 to 700 m, where the H/V technique significantly underestimated the thickness of the landslide deposits. Reasons for this could be noise from surface runoff close to stations 8, 9 and 10, which eroded the quality of recording in those stations. Despite this, the H/V method could still be considered a

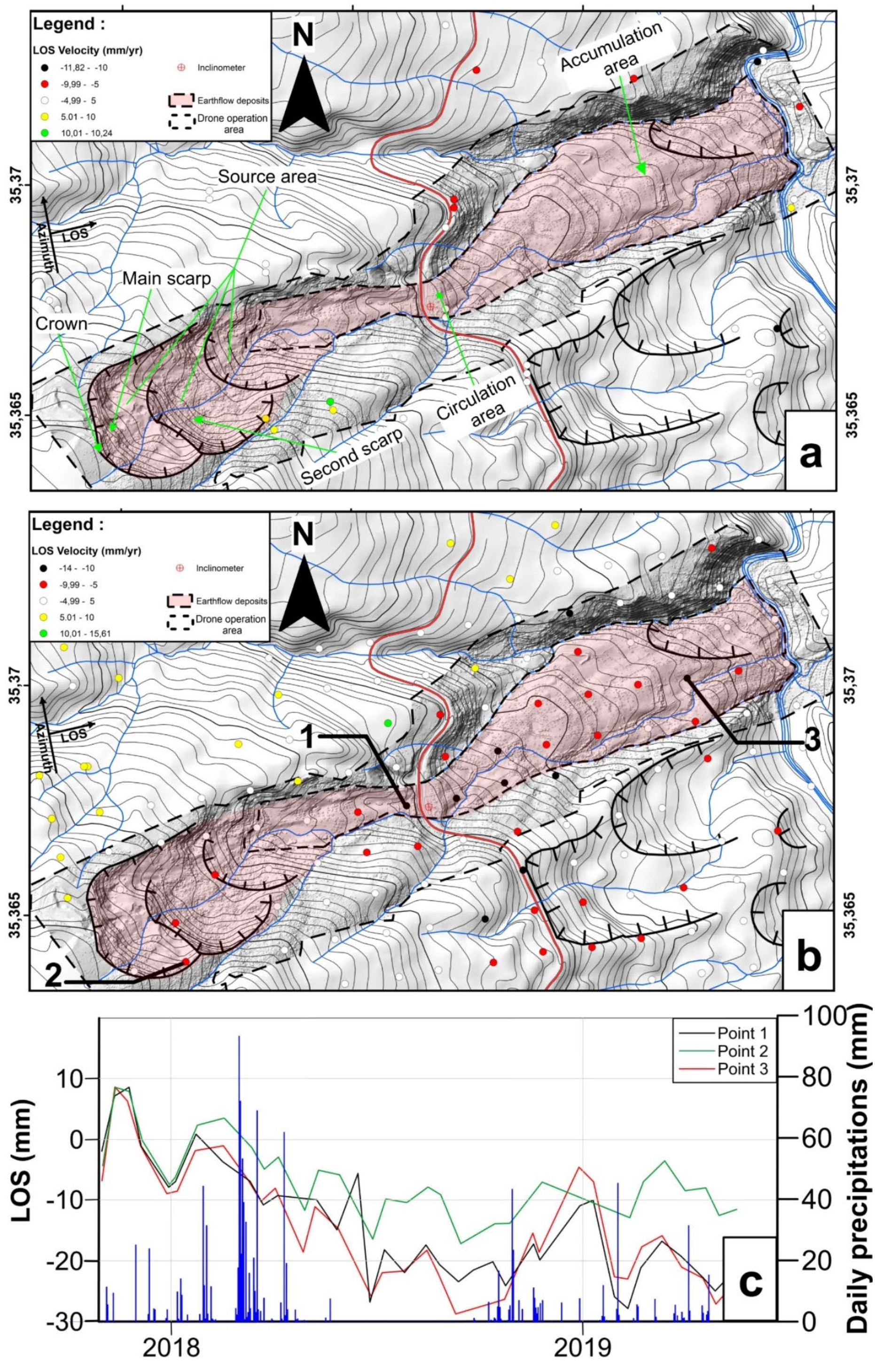

Fig. 7 Multi-date inSAR monitoring over Seikha landsldie. **a** PSinSAR results. **b** SBASinSAR results. **c** SBAS time-series plotted against daily precipitation data

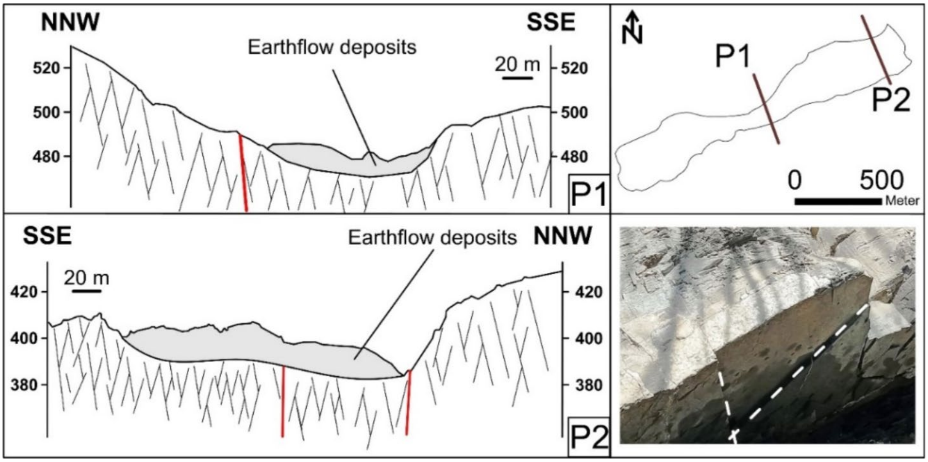

Fig. 8 Schematic transverse cross sections and field example, showing geological structures controlling the earthflow processes

good tool for studying the geometry of landslides. One of its main limitations though is the need for reference points or a third-party method to calculate V_s. In general, this need for calibration of the results is one of the main drawbacks of geophysical methods (Jongmans and Garambois 2007).

Compared to PSinSAR results presented by (Fonseca 2014), the current study constitutes a significant enhancement in terms of PS density. In effect, our results showed that the deformation is greater in the main track area in comparison to the other areas of the Seikha landslides, which cannot be achieved with low density measurements..

In addition, the displacement rates measured using SBAS interferometry are in agreement with inclinometer data, attesting their high reliability and accuracy,. Other validation tests performed on the PSinSAR and SBAS inSAR using other reference methods proved the robustness of this approach in different circumstances (Klemm et al. 2010; Peltier et al. 2010; Khorrami et al. 2020).

5.2 The complex gravitational processes of the Seikha earthflow

Although the presence of fine-grained material is the most important predictor for earthflows (Handwerger et al. 2015), the presence of folds and faults also controls the evolution of this type of instability (Pettinga 1987; Guzzetti et al. 1996; Prager et al. 2009; Pinto et al. 2016). In the Rif chain, (El Kharim 2002) and (Fonseca 2014) already established a statistical link between oriented distributions of landslides and major thrust faults that border the N-S oriented DEF unit. This spatial correlation was later investigated by Bounab (2022) who established an explanatory model for the triggering and evolution of such processes. However, a few hundreds of meters away from these major tectonic structures, the effects of the hydrogeological and lithological contrast induced by the overlapping of geologically heterogeneous terrains, diminish greatly (Supplementary, Fig. S4). In consequence, high angle strike-slip faults and tectonic joints play a more vital role in determining the shape of the landslides. Although the main axis of landslides in DEF is roughly oriented E-W to

ENE-WSW due to the elongated shape of the DEFs (Fig. 4, Supplementary, Fig. S4), the width of the landslides and its location are impacted by the presence of lithological heterogeneities and/or high-angle faults. Such a passive role of tectonic structures is demonstrated.

At the source and the depositional areas, where past accelerations occurred from 1955 to 1965, the higher percentage of clayey lithofacies facilitates the earthflow enlargement processes. However, the presence of phtanite layers, thickened by the anticline fold at the main track area constitutes an obstacle to the earthflow mass. This results in the accumulation of material and stress in this tight section of the landslide (i.e. the main track area), where internal shear is observed. A similar relationship is reported by Pinto et al. (2016) who exposed the correlation between lithological variations and gravitational deformation styles at the Montaguto landslide, Southern Italy.

Analysis of the tectonic fabric of the Seikha hillslope as a whole exposes the presence of a dense conjugate joints system controlling the earthflow direction. 2D cross sections (P1 and P2, Supplementary, Fig. S3), illustrate this relationship where the jointing system acts as a lateral slip surface, which initiated the earthflow processes.In the field, this situation can clearly be observed where the jointing segments the bedrock into small fragments, the longitudinal axis of which is parallel to the direction of the elongation stress. Subvertical strike-slip faults are also “guiding” the earthflow deposits downhill and constitute weakness areas which can be exploited by surface and subsurface water drainage and cause further enlargement of the landslide.

The presence of such fault was clear in the ERT profile traversing the depositional area (P8), (Fig. 9). In fact, an area of lower resistivity is detected below a depth 20 m (below the slip surface), which corresponds to fractured material. Its low resistivity is caused by water infiltration through the triturated material alongside a strike slip faults (Fig. 9).

The geomorphological interpretation of the longitudinal ERT profiles (Fig. 10) yields a good understanding of the landforms, landslide processes and genetic characteristics of the Seikha landslide. In the depletion area, the stretching which creates a stepped terrain morphology uphill, acts as a driving force that pushes the earthflow deposits downslope. Downhill, the internal shear forces generate a bumpy topography in the depositional area and constitute a resisting force, which slows down the material sliding along the basal slip surface. This disposition, which is concordant with the earthflow mechanical models presented by Savage and Smith (1986), Baum and Fleming (1991), Guerriero et al. (2014) and Revellino et al. (2021), makes the Seikha landslide prone to long-term instability. This is due to the fact that landslides where translational sliding is the dominant mode could be partially or totally reactivated by above-average precipitations or anthropogenic modifications

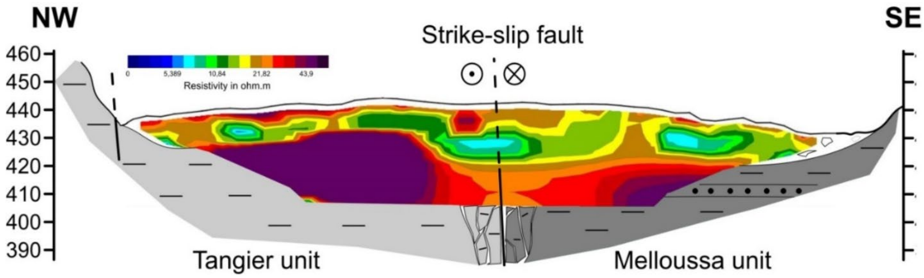

Fig. 9 Geological interpretation of the transverse 2D ERT profile (P8), showing the position of the buried strike-slip

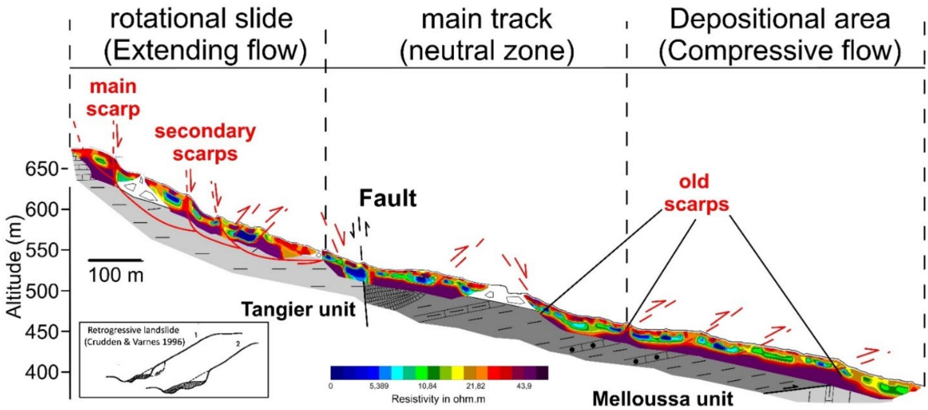

Fig. 10 Geological interpretation of the synthetic longitudinal 2D ERT profile, featuring the earthflow mechanical model and internal deformation processes

to the topography and surface/subsurface hydrology (Keefer and Johnson 1983; Skempton et al. 1989). Nevertheless, it is important to point that in our case study, no pure extension in the crown or pure compression in the depositional area is perceived in the proposed mechanical model (Fig. 10). It is in fact more similar to the model obtained by Prokešová et al. (2014) which opts for a more complicated pattern of displacement where stretched and contracted areas alternate alongside the landslide' longitudinal profile. Despite this, we see that extension and compression constitute the dominant deformation modes uphill and downhill respectively, which indicates that by and large, the Baum and Fleming (1991) model is applicable on the Seikha earthflow.

In addition, the irregular morphology of the separation surface indicates the presence of previous landslides, the scarps of which are buried under the earthflow deposits. This highlights the retrogressive and multigenerational character of the Seikha earthflow, which is impacted by the recurent activity of complex landslides evolving on the opposite wall of the DEF valley (Supplementary, Fig. S5). Consequently, one could say that the ERT technique is not only useful for studying the geometry of a given landslide, but can also reveal information regarding its genetic processes. Similar conclusions were drawn by other authors who used this method for such purposes (Falae et al. 2019; Samodra et al. 2020). In the case of Seikha earthflow, retrogressive landslides are triggered by fluvial undercutting in the western wall of the DEF interlocking spurs landforms, possibly in relation to quaternary baseline fall episodes described by El Kadiri et al. (2010). The landslide evolved to finally trigger larger processes uphill which spread into an earthflow (Supplementary, Fig. S5). Similar dynamics are reported by (Corsini et al. 2009) in a similar geomorphological context.

5.3 The trigger-failure relationship in Seikha earthflow

Being a Coulomb-plastic material, earthflow deposits are sensitive to variations of surface hydrology input, which increase pore pressure in the basal sliding surface, thus causing the partial or total reactivation of the landslide (Keefer 1977; Baum et al. 2003). In our estimation, current climate conditions manifested by the recorded rain events of the last century are

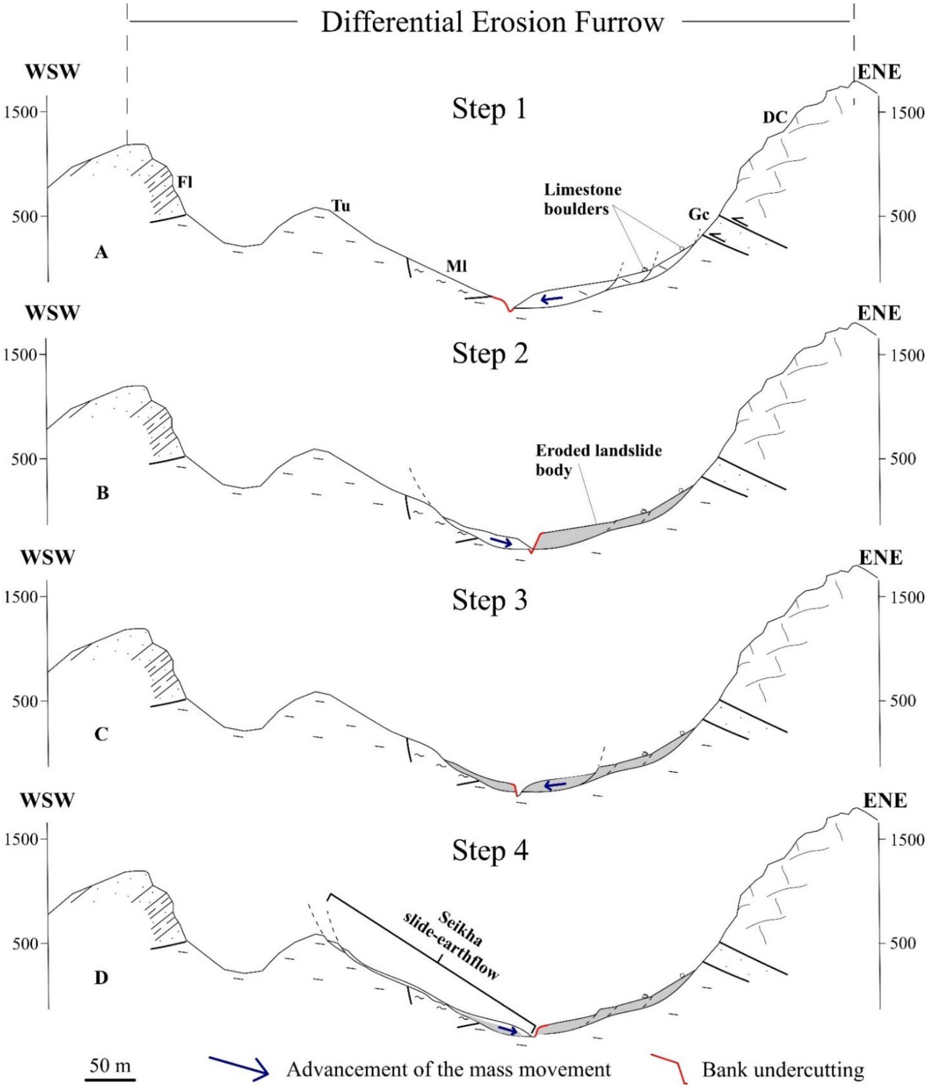

Fig. 11 Geomorphological evolution model of the DEF in relation to slope dynamics at the Seikha site. Fl - Flusch units, Tu - Tangier unit. Ml - Melloussa unit. Gc - Tertiary material of the Dorsal Calcaire unit. DC - Carbonate rocks po the dorsale calcaire unit

not sufficient to trigger large scale earthflow processes such as those observed in the Seikha landslide. In fact, such processes can only be triggered in wetter climatic conditions similar to those that characterized the Maghreb region in the early Quaternary era (Milliés-Lacroix 1965; Rognon 1987). However, during MIS-1 (i.e. the Holocene), Northern Morocco was subject to rapid climate change, characterized by pervasive millennial scale variability and abrupt centennial and decadal variations, with three main cooling periods marked by glacier advance and arid conditions (Fletcher and Zielhofer 2013). In between these periods which were dated back to 6−5 Ky before present (B. P.), 3.5–2.5 ky B. P. and 650−70 year B.P., wetter conditions are reported by these authors which could also lead to partial or total reactivation of landslides as well as episodes of intense water erosion and baselevel fall. With anthropogenic effects on the density of vegetation being obvious in the DEF area since the mid-Holocene (Abel-Schaad et al. 2018; Muller et al. 2022), the consequences of wet episodes became more pronounced in the narrow V-shaped valleys of this geomorphological unit. In this respect, some processes could be younger than MIS-5 and only date back to this period of human intervention such as the Seikha landslide, the geomorphological features of which show its relatively younger age compared to processes in the Eastern flank of the valley. In any case, radiometric dating of landslide masses in the area is crucial to determine the exact dates of occurrence of each generation of landslides at the DEF, as well as linking these processes to major climate events.

The recent deformation rates calculated using ground measurement and remote sensing techniques puts the Seikha landslide in the extremely slow category of the Cruden and Varnes (1996) classification. However, it is known that large scale earthflow processes are characterized by long term (hundreds to thousands of years) and short-term (a few years to a few tens of years) cyclic trends related to multiannual climatic cycles and/or episodes of base level fall (Mackey and Roering 2011; Delong et al. 2012). This situation can be seen in Supplementary, Fig. S3, where a succession of multiannual rainy periods that lasted from 1954 to 1970, was responsible for several partial acceleration events. After that, no significant deformation was observed.

Earthflow processes are also known to follow seasonal cyclic trends that are related to seasonal rainfall variations (Iverson and Major 1987; Mackey and Roering 2011; Corsini et al. 2015). However, the effect of the latter is not significant enough to cause long term acceleration periods. In our case study, this situation is seen in (Fig. 7c) where 3 consecutive rainy months only caused a slight acceleration of the displacement rates at the main track and depositional areas.

In fact, it is known that rainfall is responsible for increasing pore pressure, hence causing slope instability (Iverson and Major 1987; Schulz et al. 2009; Bogaard and Greco 2015). However, in our case study, the landslide's response to precipitation events was not immediate despite the emergence of aquifer water during this period, which indicates aquifer saturation (Fig. 2). In fact, it took approximately a month for ground water recharge to significantly increase pore pressure at the basal slip surface and cause an acceleration of the landslide displacement rate. A similar delay for ground water recharge (2–4 months) was reported by Prokešová et al. (2013). Reasons for this are the relatively long periods (several weeks to several months) needed for large scale complex landslides to reach their critical rainfall conditions (Zêzere et al. 2015).

6 Conclusion

The investigation conducted in this study allowed characterizing the major geomorphological processes controlling the evolution of the Seikha landslide in its geomorphological context. At the exception of the ERT and Borehole inclinometer techniques, which could prove to be labor extensive and time consuming, all data, techniques and material used in this study are low cost and time saving.

The results showed a good correlation between lithological variations, the geometry of tectonic structures and the slope instability processes. Field investigations, coupled with ERT and BI showed that the Seikha landslide follows the mechanical model of a typical terrestrial style earthflow. Regarding the landslides displacement, results of this study prove that the kinematics of this earthflow, despite it being very old, follow multiannual cyclic trends and seasonal climate variations, with effects of the latter not being significant enough to cause long term rapid accelerations.

Given the findings of this research, the gravitational processes controlling the evolution of the Seikha landslide can be integrated with previous research to explain that of the DEF unit as a whole. In fact, the multigenerational landsliding activity is evident and shows an alternation of downslope deformation on one flank of the valley and bank undercutting on the other one. Different to the oriented landslide distribution that affect mainly the eastern flank of these N-S elongated valleys, the Seikha landslide and similar other processes affecting the western Flank are preferably developed near strike-slip faults or in areas with some degree of lithological heterogeneities. Still, these observations need to be validated with statistical investigations on a larger scale in order to fully characterize the effects of the above-discussed determining factors on the short and long-term stability of hillslopes at the study area.

Supplementary Information The online version contains supplementary material available at https://doi.org/10.1007/s11069-025-07303-2.

Acknowledgements Funding for this research was provided by the CNRST "Centre National de Recherche Scientifique et Technique" as part of the PPR2/205/65 project. Funding for open access publishing: Universidad de Granada/CBUA. The authors of this paper wish to express their sincere appreciation for the financial support received from these organizations.

Author contributions Ali Bounab (Field work, Design and implementation of research, data acquisition and analysis, Writing original draft of manuscript), Younes El Kharim (Conceptualization, Funding acquisition, Design and implementation of research, initial field work for in situ tests planning, Interpretation of data, Writing– review & editing of manuscript), Rachid EL Hamdouni (Conceptualization, Funding acquisition, Design and implementation of research, initial field work for in situ tests planning, Interpretation of data, Writing– review & editing of manuscript), Reda SAHRANE (Review (First round) of the manuscript and modification of the figures), Lahcen Ourdaras (Field word and data acquisition of Electrical Resistivity Tomography).

Funding Funding for open access publishing: Universidad de Granada/CBUA.

Data availability All data generated or analyzed during this study are included in this published article and its supplementary information files.

Declarations

Competing interests The authors declare that they have no known competing financial interests or personal relationships that could have appeared to influence the work reported in this paper.

Open Access This article is licensed under a Creative Commons Attribution 4.0 International License, which permits use, sharing, adaptation, distribution and reproduction in any medium or format, as long as you give appropriate credit to the original author(s) and the source, provide a link to the Creative Commons licence, and indicate if changes were made. The images or other third party material in this article are included in the article's Creative Commons licence, unless indicated otherwise in a credit line to the material. If material is not included in the article's Creative Commons licence and your intended use is not permitted by statutory regulation or exceeds the permitted use, you will need to obtain permission directly from the copyright holder. To view a copy of this licence, visit http://creativecommons.org/licenses/by/4.0/.

References

Abel-Schaad D, Iriarte E, López-Sáez JA et al (2018) Are Cedrus Atlantica forests in the Rif mountains of Morocco heading towards local extinction? Holocene 28:1023–1037. https://doi.org/10.1177/0959683617752842

Baum RL, Fleming RW (1991) Use of longitudinal strain in identifying driving and resisting elements of landslides. Geol Soc Am Bull 103. https://doi.org/10.1130/0016-7606(1991)103%3C1121:UOLSII%3E2.3.CO;2

Baum RL, Savage WZ, Wasowski J (2003) Mechanics of Earth flows. US Geol Sur, pp 1–8

Bekaert DPS, Walters RJ, Wright TJ et al (2015) Statistical comparison of InSAR tropospheric correction techniques. Remote Sens Environ 170:40–47. https://doi.org/10.1016/j.rse.2015.08.035

Benmakhlouf M (1990) Genèse et évolution de l'accident de Tétouan et son rôle transformant Au Niveau du Rif septentrional (Maroc) (Depuis l'oligocène jusqu'à l'actuel). Université Mohammed V, Faculté des Sciences

Berardino P, Fornaro G, Lanari R, Sansosti E (2002) A new algorithm for surface deformation monitoring based on small baseline differential SAR interferograms. IEEE Trans Geosci Remote Sens 40. https://doi.org/10.1109/TGRS.2002.803792

Bogaard TA, Greco R (2015) Landslide hydrology: from hydrology to pore pressure. WIREs Water 3:439–459. https://doi.org/10.1002/wat2.1126

Bonnefoy-Claudet S, Cotton F, Bard PY (2006) The nature of noise wavefield and its applications for site effects studies. A literature review. Earth-Sci Rev 79. https://doi.org/10.1016/j.earscirev.2006.07.004

Borgatti L, Corsini A, Barbieri M et al (2006) Large reactivated landslides in weak rock masses: A case study from the Northern apennines (Italy). https://doi.org/10.1007/s10346-005-0033-9. Landslides 3:

Bounab A (2022) Multi-source analysis for the study of landslides on both sides of the Northern dorsale Calcaire: cartography and modelling. Abdelmaalek Essaadi

Bounab A, El Kharim Y, El Hamdouni R, Hlila R (2021) A multidisciplinary approach to study slope instability in the Alboran sea shoreline: study of the Tamegaret deep-seated slow-moving landslide in Northern Morocco. J Afr Earth Sci 104345. https://doi.org/10.1016/J.JAFREARSCI.2021.104345

Bounab A, Agharroud K, Kharim Y, El et al (2022) The importance of investigating causative factors and training data selection for accurate landslide susceptibility assessment: the case of Ain Lahcen commune (Tetouan, Northern Morocco. 1–31. https://doi.org/101080/1010604920222028905

Brückl E, Brunner FK, Kraus K (2006) Kinematics of a deep-seated landslide derived from photogrammetric, GPS and geophysical data. https://doi.org/10.1016/j.enggeo.2006.09.004. Eng Geol 88:

Calcaterra S, Cesi C, Maio C, Di et al (2012) Surface displacements of two landslides evaluated by GPS and inclinometer systems: A case study in Southern apennines, Italy. Nat Hazards 61. https://doi.org/10.1007/s11069-010-9633-3

Candy I, Black S (2009) The timing of quaternary calcrete development in semi-arid Southeast Spain: investigating the role of climate on calcrete genesis. Sediment Geol 218:6–15. https://doi.org/10.1016/j.sedgeo.2009.03.005

Corsini A, Borgatti L, Cervi F et al (2009) Estimating mass-wasting processes in active Earth slides - Earth flows with time-series of High-Resolution DEMs from photogrammetry and airborne lidar. Nat Hazards Earth Syst Sci 9:433–439. https://doi.org/10.5194/nhess-9-433-2009

Corsini A, Mulas M, Marcato G et al (2015) Acceleration of large active earthflows triggered by massive snow accumulation events: evidences from monitoring the Corvara landslide in early 2014 (Dolomites, Italy). In: Geophysical Research Abstracts

Crosetto M, Biescas E, Dura J et al (2008) Generation of advanced ERS and envisat interferometric SAR products using the stable point network technique. Photogramm Eng Remote Sens 74. https://doi.org/10.14358/PERS.74.4.443

Cruden DM, Varnes DJ (1996) Landslide types and processes, special report, transportation research board, National academy of sciences. U S Geol Surv 247:36–75

Degroot-Hedlin C, Constable S (1990) Occam's inversion to generate smooth, two-dimensional models from magnetotelluric data. Geophysics 55. https://doi.org/10.1190/1.1442813

Delong SB, Prentice CS, Hilley GE, Ebert Y (2012) Multitemporal ALSM change detection, sediment delivery, and process mapping at an active earthflow. Earth Surf Process Landf 37. https://doi.org/10.1002/esp.2234

Didon J, Durand-Delga M, Kornprobst J (1973) Homologies geologiques entre les Deux Rives du Detroit de Gibraltar. Bull Société Géologique Fr. https://doi.org/10.2113/gssgfbull.s7-xv.2.77. S7-XV:

Didon J, Hogga A, Haddane M (2004) Carte géologique: Souk Larbaa Beni Hessane (Echelle 1/50000). Serv Géol Maroc

Duro J, Inglada J, Closa J et al (2005) High resolution differential interferometry using time series of ERS and ENVISAT SAR data. In: European Space Agency, (Special Publication) ESA SP

El Gharbaoui A (1981) La terre et l'homme dans la péninsule tingitane: étude sur l'homme et le milieu naturel dans le Rif occidental. Institut scientifique

El Kadiri K, de Galdeano CS, Pedrera A et al (2010) Eustatic and tectonic controls on quaternary Ras Leona marine terraces (Strait of Gibraltar, Northern Morocco). Quat Res 74:277–288. https://doi.org/10.1016/J.YQRES.2010.06.008

El Kharim Y (2002) Etude des mouvements de versants Dans La région de Tétouan (Rif occidental): inventaire analyse et cartographie. Abdelmaalek Essaadi

El Kharim Y, Bounab A, Ilias O et al (2021) Landslides in the urban and suburban perimeter of Chefchaouen (Rif, Northern Morocco): inventory and case study. Nat Hazards 107. https://doi.org/10.1007/s11069-021-04586-z

Falae PO, Kanungo DP, Chauhan PKS, Dash RK (2019) Electrical resistivity tomography (ERT) based subsurface characterisation of Pakhi landslide, Garhwal Himalayas, India. Environ Earth Sci 78. https://doi.org/10.1007/s12665-019-8430-x

Ferretti A, Prati C, Rocca F (2001) Analysis of Permanent Scatterers in SAR interferometry. In: International Geoscience and Remote Sensing Symposium (IGARSS)

Fletcher WJ, Zielhofer C (2013) Fragility of Western mediterranean landscapes during holocene rapid climate changes. CATENA 103:16–29. https://doi.org/10.1016/j.catena.2011.05.001

Fletcher WJ, Fernanda M, Goñi S (2008) Orbital- and sub-orbital-scale climate impacts on vegetation of the Western mediterranean basin over the last 48, 000 year. Quat Res 70:451–464. https://doi.org/10.1016/j.yqres.2008.07.002

Fonseca AF (2014) Large deep-seated landslides in the Northern Rif mountains (Northern Morocco). inventory and analysis| Request PDF

Foumelis M, Blasco JMD, Desnos YL et al (2018) ESA SNAP - Stamps integrated processing for Sentinel-1 persistent scatterer interferometry. In: International Geoscience and Remote Sensing Symposium (IGARSS)

Gaudio V, Del, Muscillo S, Wasowski J (2014) What we can learn about slope response to earthquakes from ambient noise analysis: an overview. https://doi.org/10.1016/j.enggeo.2014.05.010. Eng Geol 182:

Gracchi T, Tacconi Stefanelli C, Rossi G et al (2022) UAV-based multitemporal remote sensing surveys of volcano unstable flanks: a case study from stromboli. Remote Sens 14:2489

Guerriero L, Coe JA, Revellino P et al (2014) Influence of slip-surface geometry on Earth-flow deformation, Montaguto Earth flow, Southern Italy. https://doi.org/10.1016/j.geomorph.2014.04.039. Geomorphology 219:

Guzzetti F, Cardinali M, Reichenbach P (1996) The influence of structural setting and lithology on landslide type and pattern. Environ Eng Geosci. https://doi.org/10.2113/gseegeosci.ii.4.531. 2:

Handwerger D, Castañeda-Aguilar R, Dahl GV et al (2015) Multivariate classification for the integration of core, log and seismic data on intersecting Pre-Stack inverted 2-D seismic lines. Lublin Basin, Poland

Hooper A, Bekaert D, Spaans K, Arikan M (2012) Recent advances in SAR interferometry time series analysis for measuring crustal deformation. Tectonophysics 514–517

Hungr O, Leroueil S, Picarelli L (2014) The Varnes classification of landslide types, an update. Landslides 11

Iverson RM, Major JJ (1987) Rainfall, ground-water flow, and seasonal movement at minor creek landslide, Northwestern California: physical interpretation of empirical relations. Geol Soc Am Bull. https://doi.org/10.1130/0016-7606(1987)99%3C579:RGFASM%3E2.0.CO;2. 99:

Jongmans D, Garambois S (2007) Geophysical investigation of landslides: A review. Bull Soc Geol Fr 178

Keefer DK (1977) A model for earthflow. Géol Soc Amer Abstr Programs USA 9:1045–1046

Keefer DK, Johnson AM (1983) Earth flows: morphology, mobilization, and movement. Geol Surv Prof Pap U S

Khorrami M, Abrishami S, Maghsoudi Y et al (2020) Extreme subsidence in a populated City (Mashhad) detected by PSInSAR considering groundwater withdrawal and geotechnical properties. Sci Rep 10. https://doi.org/10.1038/s41598-020-67989-1

Klemm H, Quseimi I, Novali F et al (2010) Monitoring horizontal and vertical surface deformation over a hydrocarbon reservoir by PSInSAR. First Break 28. https://doi.org/10.3997/1365-2397.2010014

Lanari R, Casu F, Manzo M, Lundgren P (2007) Application of the SBAS-DInSAR technique to fault Creep: a case study of the Hayward fault, California. Remote Sens Env 109:20–28

Lemoine GG, Gitelson A, Adar E, Bakker JGM (1995) Water runoff monitoring in arid areas using integrated remote sensing and GIS techniques. In: International Geoscience and Remote Sensing Symposium (IGARSS)
Lermo J, Chavez-Garcia FJ (1994) Are microtremors useful in site response evaluation? Bull - Seismol Soc Am. https://doi.org/10.1016/0148-9062(95)93340-u. 84:
Li Z, Bao Z, Li H, Liao G (2006) Image autocoregistration and InSAR interferogram Estimation using joint subspace projection. IEEE Trans Geosci Remote Sens 44. https://doi.org/10.1109/TGRS.2005.860984
Loke MH, Acworth I, Dahlin T (2003) A comparison of smooth and blocky inversion methods in 2D electrical imaging surveys. Explor Geophys 34. https://doi.org/10.1071/EG03182
Mackey BH, Roering JJ (2011) Sediment yield, Spatial characteristics, and the long-term evolution of active earthflows determined from airborne lidar and historical aerial photographs, eel river, California. Bull Geol Soc Am 123. https://doi.org/10.1130/B30306.1
Manunta M, De Luca C, Zinno I et al (2019) The parallel SBAS approach for Sentinel-1 interferometric wide swath deformation Time-Series generation: algorithm description and products quality assessment. IEEE Trans Geosci Remote Sens 57:6259–6281
Marschalko M, Yilmaz I, Bednárik M, Kubečka K (2012) Influence of underground mining activities on the slope deformation genesis: doubrava Vrchovec, doubrava Ujala and Staric case studies from Czech Republic. Eng Geol 147–148. https://doi.org/10.1016/j.enggeo.2012.07.014.:
Mastere M (2011) La susceptibilité aux mouvements de terrain Dans La Province de Chefchaouen: analyse spatiale, modélisation probabiliste multi-échelle et impacts Sur L'aménagement & L'urbanisme. université de Bretagne Occidentale
Milliés-Lacroix A (1965) Les glissements de terrain, présentation D'une Carte Prévisionnelle des mouvements de masses Dans Le Rif (Maroc septentrional). Mines Géologie 27:45–54
Mooney HM, Wetzel WW (1956) The potentials about a point electrode and apparent resistivity curves for a two- three- and four-layer Earth. University of Minnesota Press
Muller SD, Daoud-Bouattour A, Fauquette S et al (2022) Holocene history of peatland communities of central Rif (Northern Morocco). Geobios 70:35–53. https://doi.org/10.1016/j.geobios.2021.12.001
Nakamura Y (1989) Method for dynamic characteristics Estimation of subsurface using microtremor on the ground surface. Q Rep RTRI Railw Tech Res Inst Jpn 30
Niethammer U, James MR, Rothmund S et al (2012) UAV-based remote sensing of the Super-Sauze landslide: evaluation and results. Eng Geol 128. https://doi.org/10.1016/j.enggeo.2011.03.012
Palacky GJ (1988) 3. Resistivity characteristics of geologic targets. Electromagn. Methods Appl. Geophys
Pazzi V, Tanteri L, Bicocchi G et al (2017) H/V measurements as an effective tool for the reliable detection of landslide slip surfaces: case studies of Castagnola (La Spezia, Italy) and Roccalbegna (Grosseto, Italy). Phys Chem Earth 98:136–153. https://doi.org/10.1016/j.pce.2016.10.014
Peltier A, Bianchi M, Kaminski E et al (2010) PSInSAR as a new tool to monitor pre-eruptive volcano ground deformation: validation using GPS measurements on piton de La fournaise. Geophys Res Lett 37. https://doi.org/10.1029/2010GL043846
Perrone A, Lapenna V, Piscitelli S (2014) Electrical resistivity tomography technique for landslide investigation: A review. Earth-Sci Rev 135
Pettinga JR (1987) Waipoapoa landslide: A deep-seated complex block slide in tertiary weak-rock flysch, Southern Hawke's Bay, new Zealand. N Z J Geol Geophys 30. https://doi.org/10.1080/00288306.1987.10427544
Pinto F, Guerriero L, Revellino P et al (2016) Structural and lithostratigraphic controls of Earth-flow evolution, Montaguto Earth flow, Southern Italy. J Geol Soc 173. https://doi.org/10.1144/jgs2015-081
Prager C, Zangerl C, Nagler T (2009) Geological controls on slope deformations in the Köfels rockslide area (Tyrol, Austria). Austrian J Earth Sci 102
Prokešová R, Medveďová A, Tábořík P, Snopková Z (2013) Towards hydrological triggering mechanisms of large deep-seated landslides. https://doi.org/10.1007/s10346-012-0330-z. Landslides 10:
Prokešová R, Kardoš M, Tábořík P et al (2014) Kinematic behaviour of a large earthflow defined by surface displacement monitoring, DEM differencing, and ERT imaging. Geomorphology 224:86–101. https://doi.org/10.1016/j.geomorph.2014.06.029
Revellino P, Guerriero L, Ruzza G, Guadagno FM (2021) Defining kinematic and evolutive features of Earth. Flows Using Integrated Monitoring and Low-Cost Sensors
Rognon P (1987) Late quaternary Climatic reconstruction for the Maghreb (North Africa). Palaeogeogr Palaeoclimatol Palaeoecol. https://doi.org/10.1016/0031-0182(87)90003-4. 58:
Rossi G, Tanteri L, Tofani V et al (2018) Multitemporal UAV surveys for landslide mapping and characterization. Landslides 15. https://doi.org/10.1007/s10346-018-0978-0
Samodra G, Ramadhan MF, Sartohadi J et al (2020) Characterization of displacement and internal structure of landslides from multitemporal UAV and ERT imaging. Landslides 17. https://doi.org/10.1007/s10346-020-01428-0

Sancho C, Arenas C, Vázquez-urbez M et al (2015) Climatic implications of the quaternary Fl uvial Tufa record in the NE Iberian Peninsula over the last 500 ka. Quat Res 84:398–414
Sasaki Y (1992) Resolution of resistivity tomography inferred from numerical simulation. Geophys Prospect 40. https://doi.org/10.1111/j.1365-2478.1992.tb00536.x
Savage WZ, Smith WK (1986) A model for the plastic flow of landslides. US Geol Surv Prof Pap 1385. https://doi.org/10.3133/pp1385
Schulz WH, McKenna JP, Kibler JD, Biavati G (2009) Relations between hydrology and velocity of a continuously moving landslide—evidence of pore-pressure feedback regulating landslide motion? Landslides 6:181–190. https://doi.org/10.1007/s10346-009-0157-4
Skakni O, Hlila R, Pour AB et al (2020) Integrating remote sensing, GIS and in-situ data for structural mapping over a part of the NW Rif belt, Morocco. Geocarto Int. https://doi.org/10.1080/10106049.2020.1852611
Skempton AW, Leadbeater AD, Chandler RJ (1989) The Mam Tor landslide, North Derbyshire. Philos Trans R Soc Lond Ser Math Phys Sci 329. https://doi.org/10.1098/rsta.1989.0088
Turner D, Lucieer A, de Jong SM (2015) Time series analysis of landslide dynamics using an unmanned aerial vehicle (UAV). https://doi.org/10.3390/rs70201736. Remote Sens 7:
Varnes D (1978) Slope movement types and processes. Spec Rep 176:11–33
Wathelet M, Jongmans D, Ohrnberger M (2004) Surface-wave inversion using a direct search algorithm and its application to ambient vibration measurements. Surf Geophys. https://doi.org/10.3997/1873-0604.2004018. 2:
Zebker HA, Villasenor J (1992) Decorrelation in interferometric radar echoes. IEEE Trans Geosci Remote Sens 30:950–959
Zebker HA, Rosen PA, Hensley S (1997) Atmospheric effects in interferometric synthetic aperture radar surface deformation and topographic maps. J Geophys Res Solid Earth 102. https://doi.org/10.1029/96jb03804
Zêzere JL, Vaz T, Pereira S et al (2015) Rainfall thresholds for landslide activity in Portugal: a state of the Art. Environ Earth Sci 73:2917–2936. https://doi.org/10.1007/s12665-014-3672-0

Publisher's note Springer Nature remains neutral with regard to jurisdictional claims in published maps and institutional affiliations.

Authors and Affiliations

Ali Bounab[1,2] · Younes El Kharim[3] · Rachid El Hamdouni[4] · Reda Sahrane[3] · Lahcen Ourdaras[3]

✉ Rachid El Hamdouni
rachidej@ugr.es

1 Multidisciplinary Research and Innovation Laboratory, FP Khouribga, Sultan Moulay Slimane University of Beni Mellal, BP. 145, Khouribga 2500, Morocco

2 Superior School of Technology, Sultan Moulay Slimane University, Fkih Ben Salah, Morocco

3 GERN, FS, Abdelmalek Essaadi University, 93030 Tetouan, Morocco

4 Civil Engineering Department, E.T.S. de Ingeniería de Caminos, Canales y Puertos, University of Granada, Campus Universitario de Fuentenueva. C/ Severo Ochoa s/n, Granada 18071, Spain